CERN Summer Student Report:
Performance of triple-GEM detectors for the ME0 station of the CMS muon system measured in test beam

Nicholas Kurth
Rowan University, Glassboro, New Jersey,
United States of America

Supervisor: Antonello Pellecchia
INFN sezione di Bari, Italy

Submitted: August 11, 2023

The following is a summary report of my work while participating in the Research Experience for Undergraduates at CERN, hosted by the University of Michigan. Under the mentorship of Antonello Pellecchia, I studied the performance of triple gaseous electron multiplier (GEM) detectors for the ME0 station of the CMS muon system as they were irradiated with a test beam at the Gamma Irradiation Facility (GIF++).

Introduction to GEMs -

As part of the high-luminosity upgrade within the Large Hadron Collider (HL-LHC), the Compact Muon Solenoid (CMS) experiment will install in the Long Shutdown 3 of the LHC a new station of gaseous electron multiplier (GEM) detectors, called ME0, in the very forward region ($2.15<|\eta|<2.8$) of the CMS muon spectrometer [1]. Triple-GEM detectors will be utilized in this location due to their excellent space resolution (order of 100 μm), good time resolution (order of 10 ns), unprecedented longevity, and good rate capability in a highly irradiated environment [2]. A triple-GEM detector is made of three GEM foils, each consisting of a thin polymer foil with a copper coating on each side, by which biconical holes are etched at a pitch of 140 μm. With the application of an appropriate potential to the electrode, a strong electric field develops within the holes that causes nearby, free electrons to drift through and gain sufficient energy to ionize molecules via collisions [3]. The cascade effect from the electron multiplication is referred to as an avalanche. A readout plane that is segmented into 384 radially distributed strips and eight partitions, each 7 cm in height, is located in the direction of the avalanche so as to collect charges and produce a signal [4]. To reconstruct the track of a passing muon in the CMS Muon system, triple-GEM detectors in ME0 will be stacked on top of one another. An ME0 stack will be made of six triple-GEM detectors.

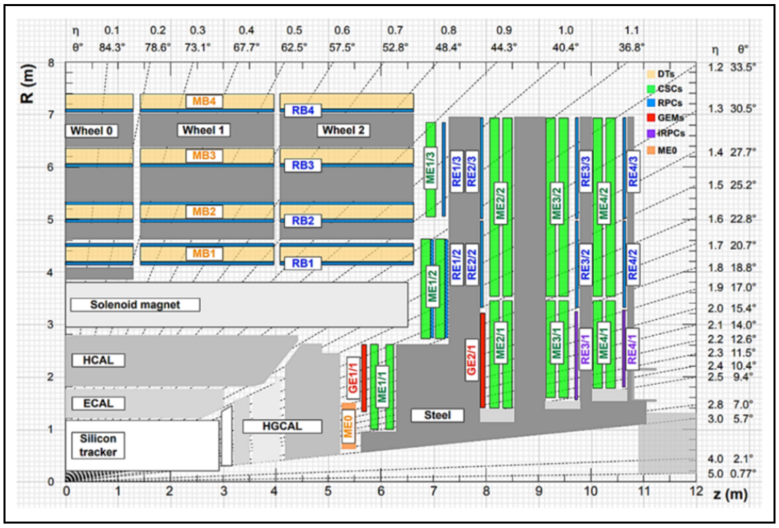

Figure 1: Quadrant of the CMS muon spectrometer, including the ME0 station upgrade (highlighted in orange) that will be installed in preparation for the HL-LHC [2].

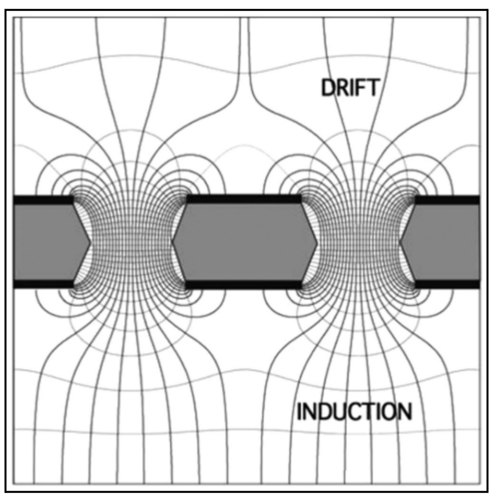

Figure 2: Electric field lines produced in the holes of the GEM electrode after the application of a potential [3].

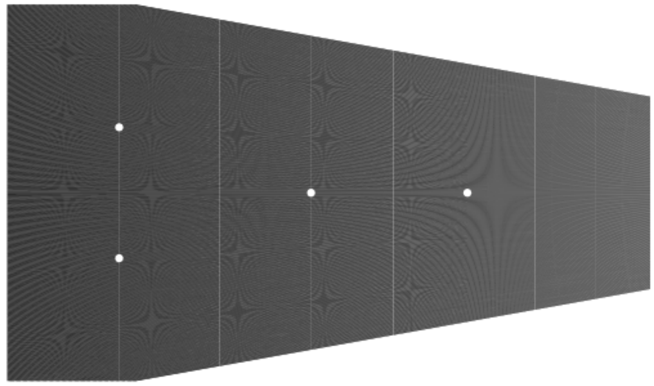

Figure 3: Design of the readout boards for the ME0 GEM detector. The segmentation along the radial direction are the strips, while the segmentation along the vertical direction are the eta partitions [4].

Basics of GEM Readout Electronics -

The front-end electronics for each GEM detector consists of a VFAT3 ASIC, an OptoHybrid concentrator board, and a GEM electronics board (GEB). The GEB is responsible for the distribution of power and electrical links among the front-end components, as well as routing induced signals on the strips to the VFAT3s. Each VFAT3 can be subdivided into an analog section made of charge-sensitive preamplifiers, a shaper and a discriminator, and a digital part responsible for buffering and communication. Data from the VFAT3s are then sent to the back-end via the OptoHybrids [4, 5]. The raw data is then sent to the data acquisition machine and stored locally for reconstruction.

Purpose -

The goal of my study was to study the performance of a ME0 stack prototype while operating in a high-background irradiation environment. Rather than the intended six detector design, the prototype consisted of four. Performance was measured at a test beam site where the detectors were irradiated with muons and their tracks could be reconstructed. The test beam was performed for two weeks at the Gamma Irradiation Facility, located at the CERN North Area on the H4 line.

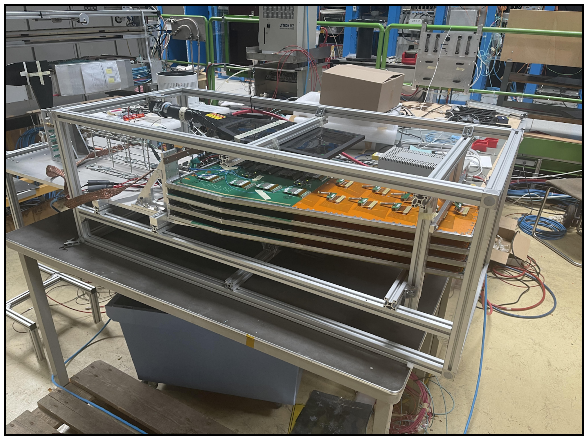

Figure 4: A prototype of the ME0 stack.

Experimental Setup within GIF++ -

The Gamma Irradiation Facility (GIF++) was established for the study of long term behavior on large gas-based detectors when placed under high-intensity background irradiation. Such studies are carried out at the facility through the mix use of a cesium-137 source, whose intensity can be adjusted with a set of attenuation filters, as well as a high energy muon beam (100 GeV/c) that is provided by the Super Proton Synchrotron. The total attenuation factor from the filters can be set to 24 different values that range from 1 (no attenuation, highest flux) to 46415 (maximum attenuation, lowest flux) [6]. During the July 2023 data collection run at GIF++, the ME0 GEM stack was located downstream and irradiated with both source and muon beam.

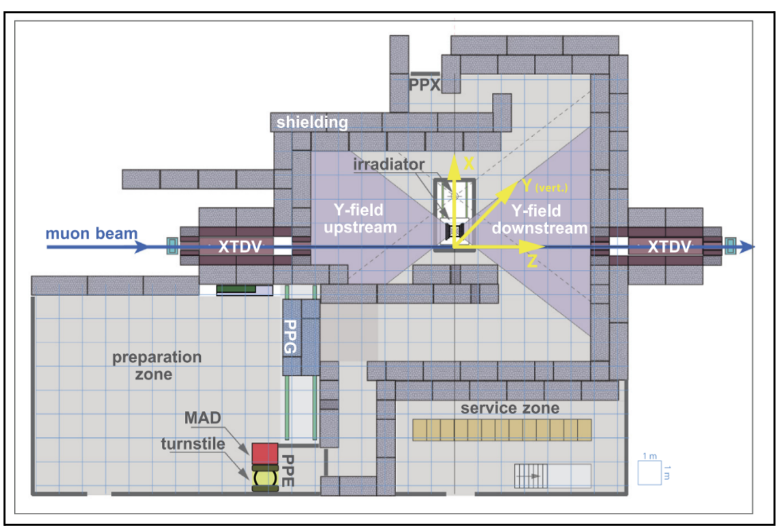

Figure 5: Layout of the GIF++ bunker [6]. Measurements of the ME0 stack during the July 2023 run were taken downstream.

Figure 6: Setup of the ME0 stack in front of the source at the GIF++.

Rate Measurements -

A rate measurement of the GIF++ source (no muon beam) was required to determine the background rate received by the detectors. The rate is calculated by counting the total number of events with a hit within a specified chamber, eta partition, or strip, *n*, over the total amount of time of the data acquisition, which depends on the total number of events during data acquisition, *N*, the pulse stretch, *p*, and the duration of 25ns of a bunch crossing [4]:

$$R = \frac{n}{N \cdot (p+1) \cdot 25ns}. \qquad \text{(Equation 1)}$$

Rate per Chamber, Eta Partition, & Strip

The rate of each run was calculated based on chamber, eta partition, and strip. As a way of determining whether a run was deemed good or not, it was expected that: chambers will have a decreasing rate as they are located further away from the source; eta partitions will have a decreasing rate as they are located further from being centered with the source; and strips should have similar rates. Misfiring strips would cause deviations from these expectations, and would be indicated by either extreme dips or peaks within the rate per strip plots.

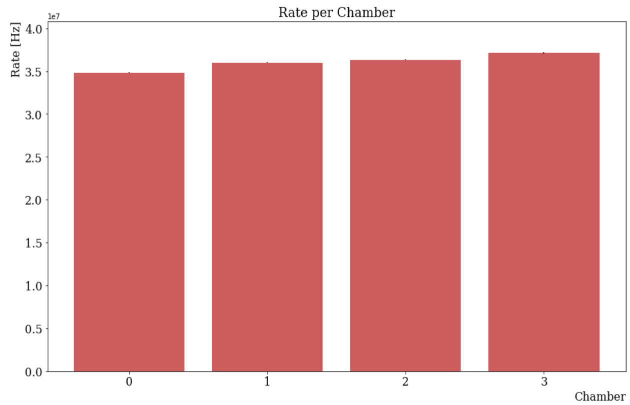

Figure 7: Typical rate distribution across all chambers. Rate decreases as the chamber is located further from the source.

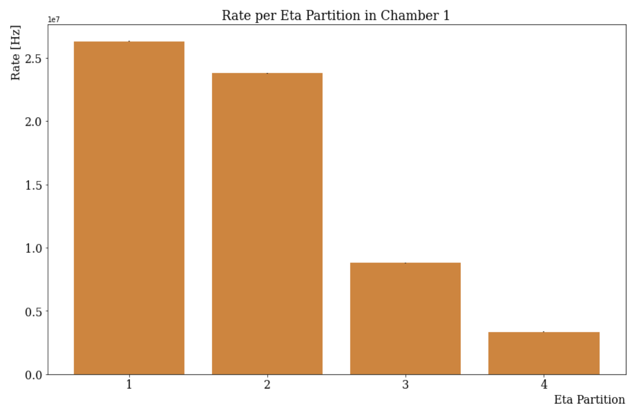

Figure 8: Typical rate distribution across all eta partitions of the same chamber. Rate decreases as the eta partition is further from being centered to the source.

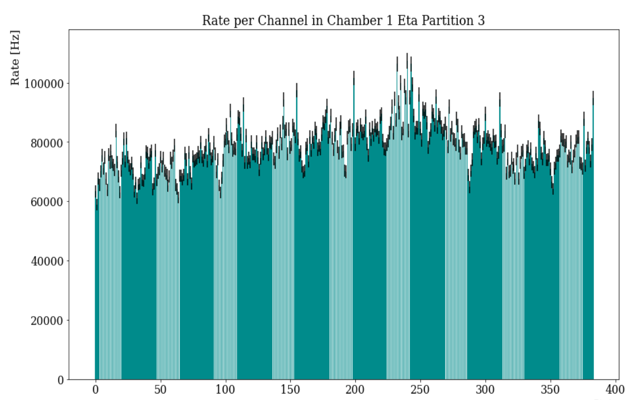

Figure 9: Typical distribution across strips of a particular eta partition.

Rate and Distance

The rate is expected to be proportional to the inverse of the distance squared from the source. However, it was found that such a relationship could not be stated with confidence due to the parameters of the experimental setup. Consider the expected relationship between rate and distance as:

$$R = \frac{C}{d^2}. \qquad \text{(Equation 2)}$$

Now consider that the chamber distances in the z-direction from the source are those provided in Table 1.

Table 1: z-Distance between chamber and source. There is a constant distance of $\Delta z = 3.5$ cm between chambers.

Chamber	z-Distance from Source [cm]
0	148.5
1	145
2	141.5
3	138

Since the chambers are evenly spaced from one another and that they are located a considerable distance from the source, Equation 2 appears to be linear rather than non-linear. This is further corroborated by the fact that when Equation 2 is Taylor expanded about a point *b*, where *b* is a point along the z-axis in the vicinity of the chamber, it is found that:

$$R = \frac{C}{b^2} - \frac{2C(x-b)}{b^3}. \qquad \text{(Equation 3)}$$

Higher order terms greater than one were excluded because of their negligible impact to the Taylor expansion's ability in modeling Equation 2. Considering that *C* and *b* are constants, it can be seen that Equation 3 simplifies to a linear equation. For these reasons, both a simple linear equation and Equation 3 were used in fitting the rate measurement.

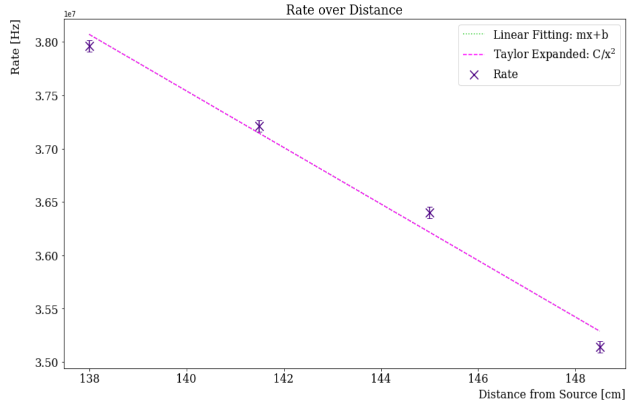

Figure 10: Rates at different distances from the source.

Rate and Attenuation

The rate was measured at varying attenuation factors, *ABS*, so as to test the detectors at varying fluxes of gamma rays from the source. Overall, the rate is proportional to the logarithmic inverse of the attenuation until the attenuation is equal to 10. After this factor, the relationship becomes nonlinear, meaning that at high fluxes the detectors lose efficiency. Chamber rates saturated greater than the eta partition rates because of the increased susceptibility to multiple hits at once due to the greater area with the same time for readout.

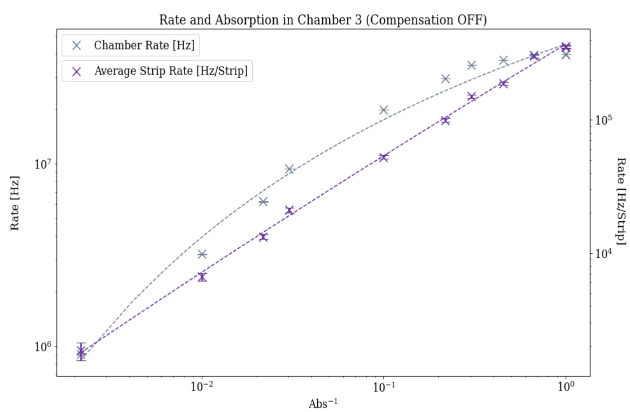

Figure 11: Chamber rate at different attenuation factors. Data fitted with $\frac{mx+b}{1+\tau(mx+b)}$ to show saturation.

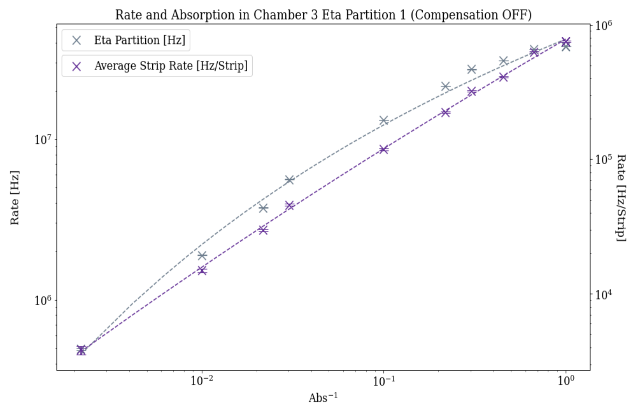

Figure 12: Eta partition rate at different attenuation factors. Data fitted with $\frac{mx+b}{1+\tau(mx+b)}$ to show saturation.

Rate and Pulse Stretch

The pulse stretch refers to the number of bunch crossings a signal is extended in time after being discriminated and synchronized with the LHC clock set at 40 MHz [4]. The rate is inversely proportional to the pulse stretch as expected by Equation 1. While fitting, an extra term was included in the denominator namely to avoid dividing by 0; however, it was found that such a term was needed as it represents the extreme limit for data collection. If it was not for the limitation in data collection technology, having a pulse stretch equivalent to -1 would allow for the recording of all incident events. A strong relationship was expected and found between chamber rate and pulse stretch as the former is larger in area and has greater susceptibility to experiencing multiple hits at once. By decreasing the pulse stretch, a chamber is better able to discern separate hits from one another.

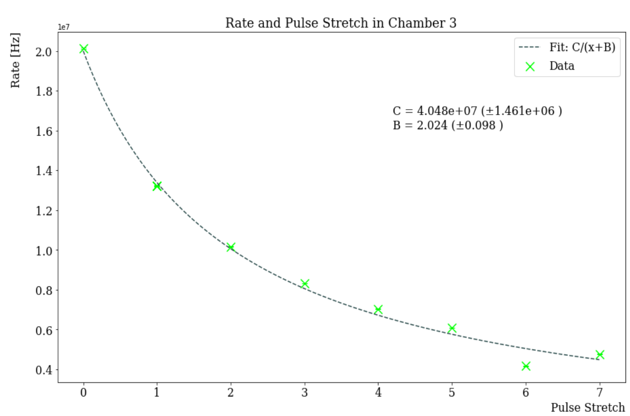

Figure 13: Chamber rate at different pulse stretches.

Spatial Resolution & Efficiency -

Tracks of muons are reconstructed by first determining the positions of hits on the detector — such hits are called reconstructed hits. From the hit positions, the following procedure takes place for each event:

1. A chamber is selected as the test;
2. Using the hits on the other chambers, a track is built using a linear fit. If multiple possible tracks exist as a result of noise, the track with the the lowest chi-squared is accepted as the true muon track while the others are discarded; lastly,
3. The position of the hit on the test chamber is extrapolated from the accepted track — such position is called the propagated hit [4].

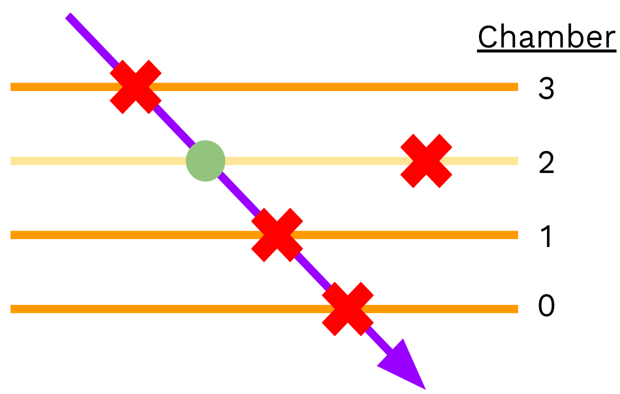

Figure 14: Simplified schematic of muon track construction where chamber 2 is selected as the test. “X” indicates the reconstructed hits, the purple line represents the accepted track, and the green dot represents the propagation hit.

The spatial resolution refers to the precision with which the position of the passing muon is reconstructed. This is done on an eta partition basis and is determined by calculating the residual difference between the propagated hit and the reconstructed hit, fitting a Gaussian curve to a histogram of the residuals, and interpreting the sigma as the spatial resolution. The theoretical spatial resolution is calculated as the strip pitch of the eta partition divided by $\sqrt{12}$; however, the actual spatial resolutions were found to be higher than the expected values [5].

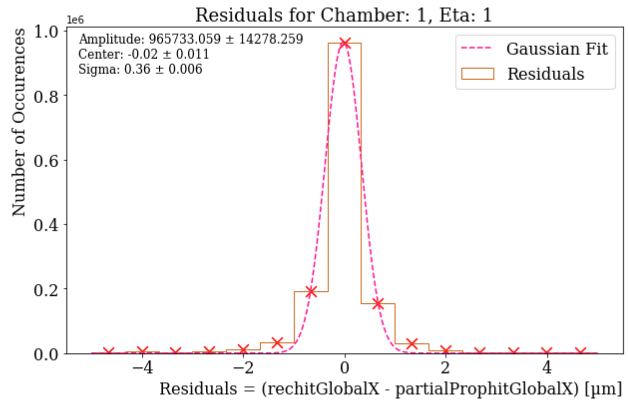

Figure 15: Distribution of residual fitted with a Gaussian curve.

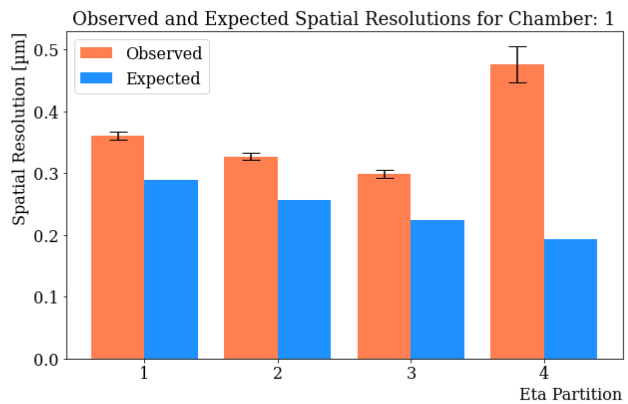

Figure 16: Comparison between the observed and expected efficiencies across different eta partitions in chamber 1.

The detector efficiency is defined as the ratio between the number of events, n, in which there is at least one reconstructed hit with a residual lower than i times the residual sigma over the total number of events, N, containing a muon track passing through the detector region [4]:

$$e = \frac{n_{<i\cdot\sigma}}{N}. \quad \text{(Equation 4)}$$

An exponential function can then be fitted with respect to the efficiency and the number of residuals used. A 5-sigma efficiency of 96.6% and an asymptotic efficiency of 97.8% were found. The latter is greater because of the background noise and is an overestimation of the efficiency.

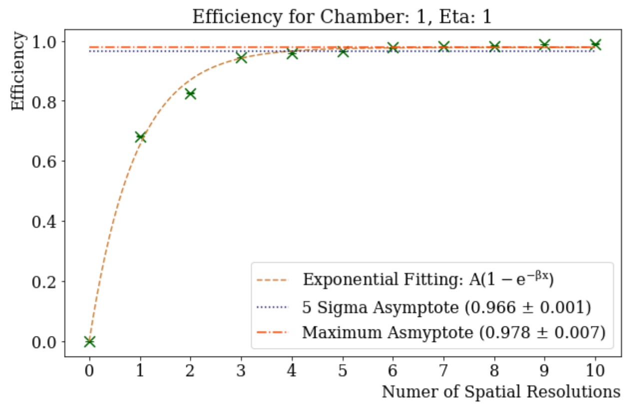

Figure 17: Efficiency of chamber 1, eta partition 1 fitted with an exponential function.

Conclusion -

The test beam further proved the great performance of triple-GEM detectors. The rate measurements followed expectations across different parameters; and though the actual spatial resolutions did not equal the theoretical values, the detector still operated with high efficiency. Future work could look into the mapping of efficiencies across eta and phi partitions and the changes in spatial resolution based on cluster size.

Acknowledgments -

I would now like to take this time to acknowledge those who provided support throughout my experience here at CERN:

- First and foremost, the greatest thanks and appreciation goes to Antonello Pellecchi for all his guidance and knowledge about GEM technology, CERN, and traveling Europe;
- To everyone who is a part of the GEM lab group… you all are amazing;
- To Myron Campbell, Junjie Zhu, Steven Goldfarb, and the Physics Department at the University of Michigan for making this experience possible;
- To Nathaniel Nucci, Gabriela González, and Eduardo Flores for providing ongoing mentorship as I navigate my physics career; and finally,
- To Josh and all the friends and family back home.

References -

[1] Colaleo, A., Safonov, A., Sharma, A., & Tytgat, M. (2015). CMS Technical Design Report for the Muon Endcap GEM Upgrade.

[2] Bianco, M., Fallavollita, F., Fiorina, D., Pellecchia, A., Ramirez, L.F., Rosi, N., & Verwilligen, P. (2022). Rate capability of large-area triple-GEM detectors and new foil design for the innermost station, ME0, of the CMS endcap muon system.

[3] Sauli, F. (2015). The gas electron multiplier (GEM): Operating principles and applications.

[4] Pellecchia, Antonello. (2023). Performance of micro-pattern gaseous detectors at the LHC and future collider experiments [Doctoral thesis, Università degli Studi di Bari Aldo Moro].

[5] Pellecchia, A., Verwilligen, P., & Stamerra A. (2022). Performance of triple-GEM detectors for the CMS Phase-2 upgrade measured in test beam.

[6] Pfeiffer, D., Gorine, G., Reithler, H., Biskup, B., Day, A., Fabich, A., Germa, J., Guida, R., Jaekel, M., & Ravotti, F. (2017). The radiation field in the Gamma Irradiation Facility GIF++ at CERN.